HHS Public Access

Author manuscript

Cortex. Author manuscript; available in PMC 2018 November 01.

Published in final edited form as:

Cortex. 2017 November ; 96: 1–18. doi:10.1016/j.cortex.2017.08.031.

Linking left hemispheric tissue preservation to fMRI language task activation in chronic stroke patients

Joseph C. Griffis[1], **Rodolphe Nenert**[2], **Jane B. Allendorfer**[2], and **Jerzy P. Szaflarski**[2]

[1]University of Alabama at Birmingham Department of Psychology

[2]University of Alabama at Birmingham Department of Neurology

Abstract

The preservation of near-typical function in distributed brain networks is associated with less severe deficits in chronic stroke patients. However, it remains unclear how task-evoked responses in networks that support complex cognitive functions such as semantic processing relate to the post-stroke brain anatomy. Here, we used recently developed methods for the analysis of multimodal MRI data to investigate the relationship between regional tissue concentration and functional MRI activation evoked during auditory semantic decisions in a sample of 43 chronic left hemispheric stroke patients and 43 age, handedness, and sex-matched controls. Our analyses revealed that closer-to-normal levels of tissue concentration in left temporo-parietal cortex and the underlying white matter correlated with the level of task-evoked activation in distributed regions associated with the semantic network. This association was not attributable to the effects of left hemispheric lesion or brain volumes, and similar results were obtained when using explicit lesion data. Left temporo-parietal tissue concentration and the associated task-evoked activations predicted patient performance on the in-scanner task, and also predicted patient performance on out-of-scanner naming and verbal fluency tasks. Exploratory analyses using the average HCP-842 tractography dataset revealed the presence of fronto-temporal, fronto-parietal, and temporo-parietal semantic network connections in the locations where tissue concentration was found to correlate with task-evoked activation in the semantic network. In summary, our results link the preservation of left posterior temporo-parietal structures with the preservation of task-evoked semantic network function in chronic left hemispheric stroke patients. Speculatively, this relationship may reflect the status of posterior temporo-parietal areas as cortical and white matter convergence zones that support coordinated processing in the distributed semantic network. Damage to these regions may contribute to atypical task-evoked responses during semantic processing in chronic stroke patients.

Keywords

stroke; aphasia; multimodal data fusion; mcca; joint ICA

Corresponding Author Information: Joseph C. Griffis, (joegriff@uab.edu), Department of Neurology and UABEC, University of Alabama at Birmingham, 312 Civitan International Research Center, 1719, 6th Avenue South, Birmingham, AL 35294-0021.

1. Introduction

Functional neuroimaging studies have enabled important insights into how post-stroke language abilities relate to the task-evoked responses of surviving brain regions (Crinion and Leff, 2007; Heiss and Thiel, 2006; Saur and Hartwigsen, 2012), and indicate that the preservation/restoration of function in pre-existing, or canonical, language networks is likely important for optimal language outcomes after left hemispheric stroke (Fridriksson et al., 2012; Griffis et al., 2017b; Heiss et al., 1999; Karbe et al., 1998; Saur et al., 2006; Szaflarski et al., 2013; van Oers et al., 2010; Winhuisen et al., 2005). If canonical language networks are not recoverable, then compensation via un-damaged right hemispheric areas is thought to underlie residual language abilities (Forkel et al., 2014; Hamilton et al., 2011; Heiss and Thiel, 2006; Saur and Hartwigsen, 2012; Turkeltaub et al., 2011). The nature of compensation afforded by right hemispheric regions is poorly understood, but recent evidence suggests that it is likely more complex than a simple take-over of the damaged areas by right hemispheric homologues (Griffis et al., 2017b; Sims et al., 2016; Laura M Skipper-Kallal et al., 2017; Laura M. Skipper-Kallal et al., 2017; Turkeltaub et al., 2012), and that it may depend on factors such as the pre-existing structural properties of the right hemisphere (Forkel et al., 2014) and the stage of recovery (Heiss and Thiel et al., 2006; Bartolomeo and de Schotten, 2016). Further, although extensive left hemispheric damage might be expected to result in prolonged dysfunction in canonical language networks (Heiss and Thiel, 2006), this may not always be the case (Griffis et al., 2017b). Thus, the recovery of function in canonical networks may depend more on the preservation of specific regions and/or connections than on the overall amount of tissue spared (Bartolomeo and de Schotten, 2016). Thus, an important question is “How do the regions recruited by chronic stroke patients during language task performance relate to the sparing vs. lesioning of different left hemispheric structures?”

Relatively few studies have explicitly investigated how language task-evoked activation relates to the status of left hemispheric brain structures in stroke patients. While most such studies have compared task-evoked activation between groups with vs. without damage to a target brain region(s) (Blank et al., 2003; Blasi et al., 2002; Heiss et al., 1999; Specht et al., 2009; Turkeltaub et al., 2011), some recent studies have used less constrained approaches that include lesion-symptom mapping of task activation (Fridriksson et al., 2010; Skipper-Kallal et al., 2017b), correlating regional activation with measures of tissue preservation/damage (Griffis et al., 2017b; Sims et al., 2016; Skipper-Kallal et al., 2017a), and joint independent component analysis of lesion and activation data (Abel et al., 2015; Specht et al., 2009). While only a minority of this work has focused on how activity in preserved left hemispheric areas relates to brain structure, the recruitment of perilesional areas during naming tasks has been previously suggested to depend on the preservation of left inferior frontal cortex (Fridriksson et al. 2010). More recently, language task-evoked activation in the left middle/superior frontal gyri and anterior cingulate cortex was reported to negatively correlate with the amount of spared tissue in posterior language areas (Sims et al., 2016). While several studies have found evidence for increased task-evoked activity in right hemispheric homologues of damaged cortical areas (Blank et al., 2003; Blasi et al., 2002; Heiss et al., 1999; Specht et al., 2009; Turkeltaub et al., 2011), increases in activation have

been reported in other areas as well (Heiss et al., 1999; Sims et al., 2016; Skipper-Kallal et al., 2017b; Specht et al., 2009), and a recent study reported decreased naming-related activation in right hemispheric homologues of damaged pre-frontal areas (Skipper-Kallal et al., 2017a). Thus, it remains unclear how the areas recruited during language task performance relate to left hemispheric brain structure. A lack of consensus among previous studies may stem in part from common limitations such as small sample sizes (i.e. n=7–15 per group) (Abel et al., 2015; Blank et al., 2003; Blasi et al., 2002; Fridriksson et al., 2010; Heiss et al., 1999; Robson et al., 2016; Sims et al., 2016; Specht et al., 2009), the lack of controls for potential confounding effects of lesion size on structure-function relationships (Abel et al., 2015; Blank et al., 2003; Blasi et al., 2002; Heiss et al., 1999; Robson et al., 2016; Specht et al., 2009; Turkeltaub et al., 2011), and differences in the type of task employed, among other factors.

In addition, a previously noted drawback to the often-used approach of comparing activation between groups with vs. without damage to a target region is that it disregards within-group lesion variability, which is present even in carefully selected groups of patients (Specht et al., 2009). To overcome this limitation, several recent studies have utilized the joint independent component analysis (jICA - Calhoun et al., 2006) approach (Abel et al., 2015; Robson et al., 2016; Specht et al., 2009), which is a data-driven method that does consider within-group lesion variability and can provide information about lesion sites associated with group differences in activation (Specht et al., 2009). While jICA therefore represents an improvement over traditional approaches, it assumes that data from each imaging modality share a single mixing matrix (i.e. that the between-modality correlations for the joint components are equal to 1), which can result in sub-optimal performance when the true between-modality correlation is low, as may often be the case for real neuroimaging data (Sui et al., 2011). Other recently developed multivariate data fusion methods such as parallel ICA (Liu et al., 2009) and multimodal canonical correlation analysis (Correa et al., 2008) operate under more flexible assumptions about cross-modal relationships, and provide more accurate estimates of their strengths than jICA. However, the source separation accuracy of approaches such as mCCA may suffer when cross-modal relationships are not sufficiently distinct (Sui et al., 2011, 2010). Importantly, the potential limitations of individual approaches can be overcome by using an approach that combines mCCA and jICA in a single hybrid analysis, referred to as multimodal canonical correlation analysis + joint ICA (mCC+jICA - Sui et al., 2011). The mCCA+jiCA approach can accurately estimate the strength of cross-modal relationships, and achieves good source separation performance even in the presence of noise (Sui et al. 2011). While these properties make mCCA+jICA an attractive alternative to other methods for studying structure-function relationships, to our knowledge, no studies have applied this technique to the study of structure-function relationships in stroke patients.

Recently, we reported that task-evoked activation in the canonical semantic network (CSN) recruited by healthy individuals during auditory semantic decisions positively predicts language task performance in chronic left hemispheric stroke patients (Griffis et al., 2017b). Given that we observed only a weak negative correlation between activation in this network and total lesion volume (Griffis et al., 2017b), we were interested in whether the preservation of specific left hemispheric structures might predict activation in regions

associated with this network. While additional lesion-symptom mapping analyses of the performance data from the same patients revealed that lesions affecting the left posterior temporo-parietal cortex and the underlying deep white matter (and to a lesser extent, anterior temporal and inferior frontal areas) predicted poor performance on the in-scanner auditory semantic decision task (Griffis et al., 2017a), it remains unclear how the location of damage relates to the regions activated during task performance. Therefore, the purpose of this study was to build upon and extend our previous work by linking patterns of activation evoked during auditory semantic decisions to patterns of the preservation of left hemispheric brain structures in chronic left hemispheric stroke patients. To this end, we used mCCA+jICA to simultaneously analyze the structural and functional MRI data obtained from the 43 chronic left hemispheric stroke patients and 43 age, sex, and handedness-matched healthy controls described in our previous reports (Griffis et al., 2017a, 2017b) and characterize links between task activation and structural preservation. Like jICA, mCCA+jICA is a data-driven method that does not require *a priori* hypotheses regarding the expected cross-modal relationships prior to performing data decomposition. However, based on our previous findings, we were especially interested in identifying relationships between left hemispheric tissue preservation and task-evoked activation in regions associated with the CSN.

2. Methods

2.1 Participants

Study procedures received approval from the Institutional Review Boards of the participating institutions. Declaration of Helsinki ethics principles and principles of informed consent were followed during all study procedures. The current study utilized MRI and language data collected from 43 chronic (> 1 year) left hemispheric stroke patients and 43 healthy controls demographically matched for age, sex, and handedness as described in our previous publications (Griffis et al., 2017a, 2017b). All participants were screened to exclude individuals that had diagnoses of degenerative/metabolic disorders, had severe depression or other psychiatric disorders, were pregnant, were not fluent in English, or had any contraindication to MRI/fMRI. Participant demographics are provided in Table 1. Comprehensive patient-level data that include task performance scores and individual lesion delineations can be found in the Supplementary Material provided with our previous publication (Griffis et al., 2017b).

2.2 Behavioral data

Prior to undergoing MRI scanning, participants were administered a set of language tests that included the Boston Naming Test (BNT) (Kaplan et al., 2001), Semantic Fluency Test (SFT) (Kozora and Cullum, 1995), and Controlled Oral Word Association Test (COWAT) (Lezak et al., 1995). An auditory semantic decision task was also administered while participants were in the scanner as previously described (Griffis et al., 2017b). This task evokes activation in a highly reproducible and well-studied semantic network (Binder et al., 2009, 2008, 1999, 1997), even in clinical populations such as stroke patients (Eaton et al., 2008; Griffis et al., 2017b), making it well-suited for the purpose of this study. Briefly, this task consisted of alternating 30s blocks of semantic decision (5 blocks) and tone decision (6 blocks) conditions. During the semantic condition blocks, participants decided whether

spoken animal names met the criteria: “native to the United States” and “commonly used by humans”. During the tone condition blocks, participants decided if brief sequences of four to seven 500- and 750-Hz tones contained two 750-Hz tones. In both conditions, participants responded by pressing a button with their non-dominant hand. Before performing the in-scanner task, participants confirmed their understanding of the task by completing a test run that consisted of 5 trials from each condition. Performance data were not collected for 4 patients due to hardware problems. These patients were therefore excluded from analyses involving in-scanner performance.

Patient scores on the SFT and COWAT were highly correlated (r=0.92), and so a combined fluency measure was defined as the average of the scores on each test, as in our previous reports (Griffis et al., 2017a, 2017b). Controls performed significantly better than patients on all language measures (in-scanner semantic decision task: $t_{74.77} = 4.71$, $p<0.001$; BNT: $t_{43.38} = 6.80$, $p<0.001$; fluency: $t_{82.28} = 13.44$, $p<0.001$). Mean language task performance for each group is shown in Table 1.

2.3 Neuroimaging data collection

MRI Data collected at the University of Alabama at Birmingham using a 3T head-only Siemens Magnetom Allegra scanner consisted of a 3D high-resolution T1-weighted anatomical scan (TR/TE = 2.3 s/2.17 ms, FOV = 25.6×25.6×19.2 cm, matrix = 256×256, flip angle = 9 degrees, slice thickness = 1mm), and two T2*-weighted gradient-echo EPI pulse functional scans (TR/TE = 2.0 s/38.0 ms, FOV = 24.0×13.6×24.0, matrix = 64×64, flip angle = 70 degrees, slice thickness = 4 mm, 165 volumes per scan). MRI data collected at the Cincinnati Children’s Hospital Medical Center using a 3T research-dedicated Philips MRI scanner consisted of a 3D high-resolution T1-weighted anatomical scan (TR/TE = 8.1 s/2.17 ms, FOV = 25.0×21.0×18.0 cm, matrix = 252×211, flip angle = 8 degrees, slice thickness = 1mm) and two T2*-weighted gradient-echo EPI pulse sequence functional scans (TR/TE = 2.0 s/38.0 ms, FOV = 24.0×13.6×24.0, matrix = 64×64, flip angle = 70 degrees, slice thickness = 4 mm, 165 volumes per scan).

2.4 Structural MRI data processing

Structural MRI data were processed using Statistical Parametric Mapping (SPM) (Friston et al., 1995) version 12 running in MATLAB r2014b (The MathWorks, Natick MA, USA). For each patient, the T1-weighted MRI scan was segmented into tissue probability maps (TPMs) and normalized to MNI template space using the New Segment procedure implemented in SPM12. Lesion probability maps were created in MNI template space using a voxel-wise naïve Bayes lesion classification algorithm implemented in the *lesion_gnb* toolbox for SPM12 (Griffis et al., 2016). These maps were visually inspected and manually thresholded to produce the final lesion masks, which were then resampled to a 2mm isotropic resolution (for a more detailed description, see Griffis et al. 2017b). Figure 1A shows lesion frequencies across all 43 patients. Lesion images for individual patients can be found in the Supplementary Material of our previous publication (Griffis et al., 2017b).

Because lesion masks were not available for the healthy controls, they could not be used as structural MRI inputs for the mCCA+jICA analysis. We therefore utilized TPMs quantifying

the brain tissue probability (i.e. GM+WM) at each voxel (Lau et al., 2015), as this provided information comparable to a typical lesion mask. Importantly, standard tissue segmentation procedures may mistakenly classify lesion voxels as intact tissue (Griffis et al., 2016; Mehta et al., 2003; Seghier et al., 2008; Wilke et al., 2011), but modifying the segmentation procedure to include additional prior information about lesion voxels remedies the problem of tissue misclassification (Sanjuan et al., 2013; Seghier et al., 2008). Therefore, a second segmentation was performed for each patient that included the smoothed (8mm FWHM) lesion mask as a prior probability map for a patient-specific lesion tissue class according to a previously described procedure for iterative lesion segmentation with patient-specific priors (Sanjuan et al., 2013). Figure 1B illustrates the effect of including the lesion prior on tissue misclassification. The resulting template-normalized GM and WM maps were smoothed with a 10mm FWHM Gaussian kernel and combined to create a single probability map quantifying at each voxel the probability that it corresponded to normal brain tissue.

2.5 Functional MRI data processing

Functional MRI data were pre-processed according to a standard pre-processing pipeline as previously described (Griffis et al., 2017b). Subject-level general linear models (GLMs) were fit to the processed fMRI data (Friston et al., 1995), and contrast estimate maps quantifying the difference in HRF magnitude between the semantic decision and tone decision conditions were created for each subject as previously described (Griffis et al., 2017b). These first-level contrast estimate maps (Semantic minus Tone) were used as the fMRI inputs into the second-level mCCA+jICA. Second-level activation maps were obtained using standard (i.e. mass-univariate) second-level *t*-contrasts, and were thresholded at a voxel-wise $p<0.01$, uncorrected and a cluster-level family-wise error corrected $p<0.05$ ($k_{crit}=$ 99 voxels as determined by 1000 Monte Carlo simulations - Slotnick et al., 2003). These maps are shown for each group in Figure 1C to illustrate the group-level activation patterns detected by a standard mass-univariate analyses. Note that the maps shown in Figure 1C utilize the same information as the maps shown in Figure 2C of our previous study (Griffis et al., 2017b), and are included simply to illustrate the mass-univariate effects.

Because we used a blocked task design, we did not separately model correct vs. incorrect trials. Further, because many patients made a substantial number of errors on the semantic decision task (Table 1), restricting our analyses to only blocks with some minimum number of correct responses would require excluding a substantial portion of the data. It should therefore be understood that the activation estimates for each patient include contributions from both correct and incorrect trials, and so activations for patients with higher overall performance are expected to be more reflective of correct responses than activations for patients with poorer overall performance.

2.6 Fusion of brain tissue and task activation data

mCCA+jICA is a second-level analysis that utilizes first-level (i.e. subject-level) feature maps representing information measured by different MRI data modalities. Each subject provided a single sMRI (i.e. smoothed brain TPM) and fMRI (i.e. contrast estimate map from the first-level GLM) feature map as inputs. The mCCA+jICA was performed according to the protocol described by Sui and colleagues (2011), as implemented in the FusionICA

toolbox (available at http://mialab.mrn.org/software/fit/). A detailed discussion of the theory behind the mCCA+jICA approach can be found in the initial report by Sui and colleagues (2011).

Prior to running the analysis, the structural MRI data were masked to include only voxels that were lesioned in at least one patient (i.e. within the lesion map shown in Figure 1A), and fMRI data were masked to include only in-brain voxels (Calhoun et al., 2006). The 3D image data from each participant were reshaped into a 1D non-zero vector and stacked to form two matrices with dimensions of [N subjects] × [n voxels] per modality, and the matrices for each feature were then normalized to have the same average sum of squares as part of the standard mCCA+jICA preprocessing pipeline (Sui et al., 2011). The minimum description length (MDL) estimation tool provided in the Fusion ICA toolbox (Li et al., 2007; Sui et al., 2011) was used to determine the number of components per modality to be estimated, which was determined to be 5 per modality, although similar results were obtained when other numbers of components were used (see Supplementary Material – Supplementary Analysis 1). Singular value decomposition (SVD) was then used to reduce each dataset to 5 components (as indicated by the MDL criteria), and mCCA was applied to the dimension-reduced data to obtain the canonical variates (D_1, D_2) and associated components (C_1,C_2) (Correa et al., 2008; Sui et al., 2011). While the canonical variates linked the data from each modality via correlation, the associated component maps were expected to still contain mixtures of independent sources (Sui et al., 2011). To achieve complete source separation, joint ICA was then performed on the concatenated maps of the mCCA components, which produced a set of joint independent components (S_1,S_2) and a single mixing matrix (W) linking them back to the input maps. Separate sMRI/fMRI mixing profiles (A_1,A_2) were obtained for each joint component by taking the product of each canonical variate (D_1,D_2) obtained from the mCCA and the inverse of the mixing matrix from joint ICA (W^{-1}). The resulting mixing profiles quantified the contribution of each joint component to the data from each subject (i.e. correspond to subject-level component loadings). Statistical tests on the mixing profiles were used to (1) select components of interest, and (2) estimate the strength of the structure-function relationship captured by each joint component of interest, as described in the following sections (sections 2.7 and 2.8). The final results were obtained by averaging over 15 ICAs using the “Average ICA” option in the Fusion ICA toolbox (Meier et al., 2012; Stephen et al., 2013). A schematic outlining the mCCA+jICA approach is provided in Figure 2.

In addition, to illustrate that our results do not depend on (1) the data fusion method employed, (2) the type of structural MRI data utilized, or (3) the inclusion of data from healthy individuals, we also performed (1) a parallel ICA analysis using explicit lesion masks rather than brain tissue maps (see Supplementary Analysis 2), and (2) a multivariate lesion-symptom mapping analysis of fMRI loadings (see Supplementary Analysis 3). These analyses are presented in the Supplementary Material, and provide results that are highly consistent with the results of the mCCA+jICA approach.

2.7 Selection of group-differentiating joint components

Like jICA, mCCA+jICA does not require *a priori* hypotheses prior to data decomposition, but component selection must be justified by *a priori* hypotheses or statistical criteria. As in previous studies using similar methods to study structure-function relationships in stroke patients, joint ICs were selected for further analyses on the basis that their mixing coefficients that significantly differed between patients and controls (Abel et al., 2015; Robson et al., 2016; Specht et al., 2009). These ICs are referred to as group-differentiating joint ICs (Sui et al., 2011) because they represent structure-function profiles that are differently represented in the patient and control groups. Group differences in mixing coefficients were assessed using two-tailed independent samples *t*-tests with degrees of freedom adjusted for unequal variances. Bonferroni-Holm correction was applied to control the family-wise error rate (FWER) at 0.05 across all 10 tests (Aickin and Gensler, 1996). This revealed a total of 3 significant (i.e. FWE$p<0.05$) group-differentiating joint ICs (Figure 3) that were retained for further analyses.

2.8 Characterization of cross-modal relationships for selected components

The cross-modal connection strengths for each group-differentiating joint IC were characterized by correlating the corresponding sMRI and fMRI mixing coefficients (Sui et al., 2011). Partial correlations were used to assess whether the cross-modal connections persisted when controlling for the effects of left hemispheric brain volume and lesion volume. Left hemispheric brain volume was strongly anti-correlated with lesion volume in the stroke patients ($r=-0.86$, $p<0.001$ – patients with larger lesions had smaller left hemispheric brain volumes). Mean left hemispheric brain volumes were significantly larger in the control group ($t_{62.02}=11.18$, $p<0.001$; see Table 1 for group means).

2.9 Characterization of behavioral relationships for selected joint components

Relationships between patient mixing coefficients for the selected joint ICs and language task scores were explored with robust multiple regressions using iteratively re-weighted least squares (implemented in the MATLAB Statistics Toolbox) to reduce the influence of outlier data points and protect against false positives (Poldrack, 2012; Wager et al., 2005). For each language task, we fit an (1) sMRI model, and (2) an fMRI model. Each model included patient mixing coefficients for the 3 group-differentiating ICs from the corresponding modality (i.e. sMRI ICs for the SMRI models; fMRI ICs for the fMRI models) as predictors. Models were considered significant if the *p*-value for the *F*-test against the intercept-only model was less than 0.05, FWE-corrected for all 6 full model tests using the Bonferroni-Holm procedure. Individual predictors were considered significant if the *p*-value of the *t*-test for the parameter estimate was less than 0.10, adjusted for the false discovery rate (FDR) across all 18 individual predictor tests (Benjamini and Hochberg, 1995; Genovese et al., 2002).■■

Additional lesion size covariates were not included in the behavioral regression analyses because they were multi-collinear or close-to-multi-collinear with the sMRI predictors as indicated by variance inflation factors (VIF) of 16.95 and 8.22 for left hemispheric brain volume and lesion size, respectively (Belsley et al., 1980). Patient left hemispheric brain volumes were nearly perfectly predicted by a model including patient loadings on all three

group-differentiating sMRI ICs (R^2=0.93, p<0.001). Loadings on sMRI IC3 were the best predictor of left hemispheric brain volumes (sMRI IC1: b=0.58, t_{39}=12.49, p<0.001; sMRI IC2: b= 0.55, t_{39}=6.50, p<0.001; sMRI IC3: b=0.77, t_{39}=18.29, p<0.001). Lesion volume showed similar relationships to loadings on the group-differentiating sMRI ICs (R^2=0.88, p<0.001; sMRI IC1: b=−0.59, t_{39}=−10.43, p<0.001; sMRI IC2: b=−0.31, t_{39}=−3.01 p=0.005; sMRI IC3: b=−0.63, t_{39}=−12.39, p<0.001). However, neither left hemispheric brain volumes (R^2=0.13, p=0.14; fMRI IC1: b=0.18, t_{39}=1.87, p=0.07; fMRI IC2: b=0.22, t_{39}=1.75, p=0.09, fMRI IC3: b=0.09, t_{39}=0.72, p=0.48) nor lesion volumes (R^2=0.11, p=0.21; fMRI IC1: b=−0.14, t_{39}=−1.74, p=0.09; fMRI IC2: b=−0.14, t_{39}=−1.32, p=0.19 fMRI IC3: b=−0.08, t_{39}=−0.74, p=0.46) were significantly predicted by loadings on the group-differentiating fMRI ICs. Thus, lesion size covariates were not included in the sMRI models due to multi-collinearity, and for consistency between the sMRI and fMRI models, they were also not included in the fMRI models. Importantly, relationships between the fMRI loadings and brain volume/lesion volume measures were weak and were not statistically significant.

3. Results

3.1 Group-differentiating joint ICs

Three group-differentiating joint ICs were identified by mCCA+jICA. The control group had significantly greater mean mixing profile coefficients for sMRI IC1 ($t_{43.6}$=7.37, FWEp<0.001) and fMRI IC1 ($t_{75.41}$=5.39, FWEp<0.001), sMRI IC2 ($t_{42.66}$=7.86, FWEp<0.001) and fMRI IC2 ($t_{82.91}$=2.88, FWEp=0.025), and sMRI IC3 ($t_{45.99}$=5.83, FWEp<0.001) and fMRI IC3 ($t_{82.82}$=4.47, FWEp<0.001), indicating that these components were more strongly represented in the control data than in the patient data (see Figure 3 for group means). To visualize the voxel-level contributions to each of the group-differentiating joint components, the values in the corresponding spatial maps were converted to Z-values by dividing each voxel's value by the standard deviation of voxel values in the map and thresholded at |Z|>2.0 (Calhoun et al., 2006 Sui et al., 2011). The thresholded maps are shown in Figure 3.

The sMRI components of the group differentiating joint ICs reflected three general patterns of tissue preservation involving (1) left posterior temporo-parietal regions, (2) left basal ganglia/insular regions, and (3) left inferior frontal regions (Figure 3). The fMRI components of the group-differentiating joint ICs reflected three distinct patterns of activation, two of which (i.e. fMRI IC1 and fMRI IC3) predominantly featured regions associated with the CSN identified by the mass-univariate analysis (Figure 1C, Figure 3A,C). The first fMRI component (fMRI IC1) was the most strongly represented component in the data from both groups, as indicated by having the highest mean mixing profile coefficients for each group (Figure 3).

Spatial similarity between the CSN identified by the mass-univariate analysis (shown in Figure 1C) and each group-differentiating fMRI IC was assessed by correlating the voxel values in the unthresholded CSN t-statistic map with the voxel values in the unthresholded fMRI IC z-statistic maps. The strongest correlation was observed for fMRI IC1 (r=0.68, p<0.001), followed by fMRI IC3 (r=0.49, p<0.001), and fMRI IC2 (r=0.30, p<0.001). Based

on recent reports detailing the sub-networks of the CSN, we interpreted fMRI IC1 and fMRI IC3 as corresponding to the default mode/perisylvian and fronto-parietal network sub-networks, respectively (Xu et al., 2016). We interpreted fMRI IC2 as corresponding to a previously described bilateral sub-network primarily involving the inferior frontal gyrus pars orbitalis that is thought to primarily reflect differences in the decision-making aspect of the tasks (Kim et al., 2011).

3.2 Cross-modal connection strengths for selected components

All three group-differentiating joint ICs showed significant correlations between their fMRI and sMRI mixing profile coefficients (Joint IC1: r=0.53, FWEp<0.001; Joint IC2: r=0.33, FWEp=0.004; Joint IC3: r=0.30, FWEp=0.004). The mixing profile coefficient correlation for joint IC1 persisted when the effect of left hemispheric brain volume was held constant (partial r=0.31, p=0.004), and when this analysis was restricted to the patient group (partial r=0.33, p=0.03). A similar relationship was observed when lesion volume was held constant for the patient group (partial r=0.30, p=0.05). However, the mixing profile coefficient correlations for the other two joint ICs did not persist when left hemispheric brain volume was held constant (joint IC2: partial r=0.20, p=0.07; joint IC3: partial r=−0.03, p=0.8), remained non-significant when the analyses were restricted to the patient group (joint IC2: partial r=0.20, p=0.21; joint IC3: partial r=0.05, p=0.78), and remained non-significant when lesion volume was held constant for the patient group (joint IC2: partial r=0.24, p=0.13; joint IC3: partial r=0.02, p=0.86). Scatter plots illustrating these relationships are shown in Figure 4.

The results of the partial correlation analyses indicate that the relationship between sMRI and fMRI mixing profile coefficients for joint IC1 are not attributable to the total amount of preserved left hemispheric tissue or to lesion size. Because lesions were most frequent in the white matter underlying the left frontal operculum (Figure 1A), it is also unlikely that this relationship is driven by lesion frequency effects. Highly similar, albeit slightly stronger (r=0.47, FWEp=0.04 – corrected for 25 comparisons; partial r=0.42, p=0.008 when lesion volume was held constant), effects were obtained from the parallel ICA of lesion and task data from the patient group (see Supplementary Analysis 2). Similar results were also obtained from the lesion-symptom mapping analysis (see Supplementary Analysis 3).

3.3 Relationships between patient mixing coefficients and behavioral performance

Results from the behavioral regression analyses are presented in Table 2. All sMRI and fMRI models significantly predicted task performance. Notably, patient mixing coefficients for sMRI IC1 significantly predicted all three language outcomes in the sMRI models, consistent with our previous findings that posterior temporo-parietal lesions predicted poor performance on all 3 tasks in these patients (Griffis et al., 2017a). Patient mixing coefficients for the two most strongly represented fMRI ICs in the control data (fMRI ICs 1 and 3), which were also the most similar to the CSN identified by the mass-univariate analysis, significantly predicted all three language outcomes in the fMRI models. This was also consistent with our previous findings regarding the relationships between language task-evoked activation in the CSN and language task performance in these patients (Griffis et al. 2017b).

3.4 Exploratory fiber tracking

Recent studies indicate that posterior temporo-parietal regions (i.e. regions associated with sMRI IC1 – see Figure 3A) harbor a disproportionate number of structural connections to other language-relevant areas (Ivanova et al., 2016; Martino et al., 2013; Turken and Dronkers, 2011) and are functionally connected to other portions of the semantic network at rest (Turken and Dronkers 2011). There is also evidence that task-evoked networks strongly reflect the intrinsic functional network architecture (Cole et al., 2014), which itself reflects underlying structural connections (Honey and Sporns, 2009). Therefore, damage to the regions corresponding to sMRI IC1 might be expected to disrupt communication in the CSN by damaging structural connections, and this might be expected to produce altered task-evoked activation.

While we could not directly address this hypothesis, we performed a *post-hoc* deterministic fiber tracking analysis to explore the structural connections of the CSN associated with the regions identified by mCCA+jICA. These analyses were performed using a freely available, pre-processed, group-averaged (N=842) tractography dataset (WU-Minn HCP Consortium; HCP-842 tractography template - http://dsi-studio.labsolver.org/download-images/hcp-842-template) consisting of diffusion MRI data from the Human Connectome Project (2015 Q4, 900 subject release, 842 subjects included) that were reconstructed in MNI atlas space using Q-space diffeomorphic reconstruction (QSDR - Yeh et al., 2010; Yeh and Tseng, 2011) and averaged to create a population-level tractography template (for details, see Yeh et al., 2017). Data were accessed under the WU-Minn HCP open access agreement, and were originally acquired using a multi-shell diffusion scheme (b-values: 1000b-values: 2000, and 3000 s/mm2; diffusion sampling directions: 90, 90, and 90; in-plane resolution: 1.25mm). Because the data were already pre-processed and in MNI atlas space, no further processing was performed.

For these analyses, a broad CSN region of interest was defined as those regions identified by the mass-univariate analysis of the control data (Griffis et al. 2017b), which are shown in Figure 1C. This broader definition (i.e. as opposed to the more specific sub-networks identified by mCCA+jICA) was chosen to enable the identification of all tracts associated with the large-scale CSN. Deterministic fiber tracking analyses (Yeh et al., 2013) were performed as previously reported (for details, see Griffis et al. 2017a) using default tracking parameters in the DSI_Studio software package (http://dsi-studio.labsolver.org/) in order to identify fiber tracts that both originated and terminated within the CSN region of interest. Each of the three sMRI components of the group-differentiating joint ICs identified by the mCCA+joint ICA were thresholded ($|Z|>2.0$) and used as ROIs to retain only the tracts passing through the corresponding regions. Therefore, the resulting tracts both (1) connected different portions of the CSN, and (2) passed through the areas corresponding to the thresholded sMRI components of the group-differentiating joint ICs. These tracts were then manually separated and labeled as previously reported (Griffis et al., 2017a). This approach is analogous to other methods employed by previous studies that have characterized the structural connections of regions identified by lesion-deficit analyses (Harvey and Schnur, 2015; Mirman et al., 2015; Turken and Dronkers, 2011), and while indirect, provides

qualitative information about the expected structural connections and endpoints associated with each region identified by mCCA+jICA.

Connections passing through voxels associated with SMRI IC1 corresponded to the superior longitudinal fasciculus II, long segment of the arcuate fasciculus, posterior segment of the arcuate fasciculus, inferior fronto-occipital fasciculus, middle longitudinal fasciculus, and short-range fibers connecting the angular gyrus to the ppsterior superior temporal gyrus. Connections passing through voxels associated with sMRI IC2 consisted of the inferior fronto-occipital fasciculus, uncinate fasciculus, anterior thalamic radiations, frontal aslant tract, and short-range fibers connecting the inferior frontal gyrus pars triangularis to the anterior insula. Finally, connections with fibers passing through voxels associated with sMRI IC3 consisted of the long segment of the arcuate fasciculus, anterior thalamic radiations, frontal aslant tract, short-range fibers connecting the inferior frontal gyrus pars opercularis to the precentral gyrus, short-range fibers connecting the inferior frontal gyrus to the middle frontal gyrus, and callosal fibers connecting bilateral superior frontal gyri. These results are shown in Figure 5B. Fiber tract endpoints for the connections passing through voxels associated with each sMRI IC are shown in Figure 5C. We note that these results only represent fibers connecting regions associated with the CSN, and do not account for all fibers passing through each region. It should be emphasized that these results can only provide information the expected structural connections associated with each sMRI IC in healthy individuals (see Limitations).

4. Discussion

4.1 Semantic network activation and left hemispheric tissue preservation

Here, we characterized relationships between task-evoked fMRI activation and tissue preservation in chronic left hemispheric stroke patients using mCCA+jICA. In addition to using optimized techniques for data-driven analyses of structure-function relationships, this study featured strengths that include (1) the relatively large sample of patients and controls (n=43 per group), and (2) the use of statistical controls for confounds related to overall lesion size. Our analyses revealed an association between the status of left posterior temporo-parietal areas and the level of activation in (1) areas associated with the CSN and (2) right fronto-temporo-parietal areas. Importantly, these relationships could not be attributed to the effects of left hemispheric brain volume or overall lesion volume, and are unlikely to reflect overall lesion frequency effects. Patient loadings for both the tissue preservation and fMRI activation components of joint IC1 correlated positively with performance on in-scanner and out-of-scanner language tasks, consistent with our previous studies separately characterizing the structural and functional correlates of language task performance in this sample (Griffis et al. 2017a, 2017b). While task performance was also positively correlated with patient contributions to joint IC3, which featured fMRI activity in the left fronto-parietal sub-network of the CSN and tissue preservation in the left inferior frontal gyrus, the cross-modal relationship for this component did not hold in the patient group or when controlling for lesion size effects. Thus, while the activation pattern captured in fMRI IC3 is associated with better task performance in patients, conclusions about its relationship to brain structure are not warranted by these data. Finally, our fiber tracking

results suggest that regions corresponding to the structural component of joint IC1 likely contain diverse structural connections traversing frontal, temporal, and parietal portions of the CSN in healthy individuals. This is consistent with previous reports indicating that posterior temporal regions are traversed by multiple tracts connecting the distributed CSN (Turken and Dronkers 2011), and also supports the proposal that damage to regions containing multiple long-range fiber tracts may produce wide-spread abnormalities in network function (Griffis et al., 2017a; Ramsey et al., 2017). Thus, the preservation of left temporo-parietal regions may contribute to the preservation/restoration of CSN function in chronic left hemispheric stroke patients. We discuss these results in the context of the broader literature below.

As noted earlier, the semantic decision task used in this study has been consistently shown to produce robust activation in a bilateral but predominantly left hemispheric network that includes the inferior frontal gyrus pars triangularis, middle frontal gyrus, superior frontal gyrus, anterior temporal lobe, posterior middle temporal gyrus, angular gyrus, posterior supramarginal gyrus, precuneus, hippocampus, and posterior cingulate cortex in healthy and clinical populations (Binder et al., 2009, 2008, 1999, 1997; Donnelly et al., 2011; Griffis et al., 2017b; Kim et al., 2011; Szaflarski et al., 2008). Accordingly, robust activation in these regions was detected by the mass-univariate analysis of the fMRI data, as can be seen in Figure 1C. The structural connections supporting this network have been previously reported to include the arcuate fasciculus and inferior fronto-occipital fasciculus, and multiple relevant fiber pathways have been reported to converge in the white matter underlying posterior temporo-parietal cortical areas (Catani et al., 2012; Griffis et al., 2017a; Ivanova et al., 2016; Martino et al., 2013; Turken and Dronkers, 2011). These cortical areas, which include the posterior superior temporal gyrus, angular gyrus, posterior supramarginal gyrus, and other portions of the inferior parietal lobule, may correspond to heteromodal convergence zones that integrate modality-specific (i.e. sensory, motor, etc.) information to form and store abstract knowledge (Binder and Desai, 2011; Skipper-Kallal et al., 2015). Along these lines, recent evidence indicates that the CSN is composed of at least three sub-networks – the peri-sylvian, default mode, and fronto-parietal sub-networks – that play specialized roles in high-level language processing, semantic memory, and semantic control, respectively (Xu et al., 2016). The integration of these networks during semantic processing likely depends on cortical hub regions that include the left angular gyrus (integration of all three sub-networks), posterior supramarginal gyrus (integration within the peri-sylvian network), and inferior parietal lobule (integration of the fronto-parietal and default-mode networks) (Xu et al., 2016). Accordingly, previous evidence suggests that among regions within the left middle cerebral artery distribution, temporo-parietal areas feature disproportionate functional connections compared to lateral prefrontal areas like the inferior frontal gyrus (Buckner et al., 2009) Different portions of the temporo-parietal areas associated with the CSN also show distinct patterns of functional connectivity with other broadly specialized large-scale networks. For example, the angular gyrus is associated with the broader default-mode network, while the supramarginal gyrus is associated with the ventral attention and cingulo-opercular networks, and the inferior parietal lobule is associated with the broader fronto-parietal network (Daselaar et al., 2013; Uddin et al., 2010). Notably, these regions were included in the structural component of joint IC1

identified by mCCA+jICA (Figure 3A), the linked lesion component identified by parallel ICA (Supplementary Analysis 2), and the lesion predictors of loadings on fMRI IC1 identified by multivariate lesion-symptom mapping (Supplementary Analysis 3). To summarize, the left posterior temporo-parietal areas associated with the structural component of joint IC1 are likely convergence zones that contain white matter pathways connecting different portions of the CSN, are involved in the integration of modality-specific information from sensory/motor areas, are involved in integrating functionally distinct CSN sub-networks to accomplish semantic processing, and are associated with distinct larger-scale functional networks. These properties provide important clues as to why tissue preservation in these regions may be important for the preservation/restoration of task-evoked activation in the CSN after left hemispheric stroke.

Given that posterior temporo-parietal areas correspond to a convergence of functional and structural networks, it is possible that the observed relationship between task-evoked activation in the CSN and tissue preservation in these regions may reflect, to varying degrees, the preservation of structural pathways connecting distributed portions of the CSN, cortical regions mediating the mapping of low-level inputs to abstract concepts, cortical regions mediating the integration of sub-networks associated with the CSN to accomplish task goals, and cortical regions associated with distinct larger-scale brain networks involved in broad aspects of cognitive function. The destruction of structural connections and/or cortical regions mediating the integration of CSN sub-networks would be expected to result in aberrant task-evoked function in the CSN, and the destruction of cortical regions associated with distinct large-scale brain networks might be expected to lead to changes in the task-evoked properties of networks outside of the CSN. This point is important to consider given the opposite contributions of activity in the CSN and activity in right fronto-temporo-parietal areas to semantic decisions vs. tone decisions (Figure 1C; Figure 3A; Supplementary Figure 2). One hypothesis is that in healthy individuals and patients with preserved temporo-parietal structures, this reflects the segregation of these networks to accomplish high-level semantic (i.e. semantic decisions) vs. lower-level sensory (i.e. tone decisions) tasks; in patients with posterior temporo-parietal damage, the loss of structural connections and/or a diminished capacity for integrated network function might reduce CSN activation, while a diminished capacity for task-driven segregation between semantic vs. attention networks might increase right fronto-temporo-parietal activation.

This proposal is broadly consistent with the implications of recent reports that task-driven interactions among the default mode, left fronto-temporo-parietal, and right fronto-temporo-parietal networks during speech production are disrupted in left hemispheric stroke patients (Geranmayeh et al., 2016), namely that altered large-scale network dynamics may underlie atypical task-evoked responses in chronic stroke patients. This also implies that patients with temporo-parietal damage should show disrupted network interactions at rest in addition to changes in task-evoked network properties. While testing for these effects is beyond the scope of the current study, several lines of evidence support the plausibility of this explanation. For example, default mode hub regions are involved in modulating activity in other networks that include task-positive prefrontal networks (Uddin et al., 2009), and circumscribed lesions of the medial prefrontal cortex (a core default mode region) result in disrupted functional interactions between the default mode and attention/motor networks at

rest (Eldaief et al., 2016). Growing evidence also indicates that large-scale network interactions are disrupted in patients with post-stroke visuospatial neglect (Baldassarre et al., 2014; He et al., 2007). Severe disruptions of functional connectivity in neglect patients have previously been associated with damage to portions of the white matter harboring fibers from both the right arcuate and superior longitudinal fasciculi (He et al., 2007). Notably, the left hemispheric homologues of both of these tracts are expected to be damaged in patients with lesions resembling sMRI IC1 (Figure 5B). While this explanation of our results is therefore plausible, it is not the only explanation for the observed effects.

Another potential explanation is that dysfunction within CSN is accompanied by right fronto-temporo-parietal compensation in chronic patients. As noted in the Introduction, it is thought that right hemispheric regions may be recruited to support residual language abilities when canonical language networks are not sufficiently preserved/restored (Heiss and Thiel 2006; Hamilton et al., 2011; Turkeltaub et al., 2011, 2012; Saur and Hartwigsen 2012). Indeed, we recently reported that higher activation in several of the right frontal regions (i.e. right inferior frontal gyrus and right supplementary motor area) featured in fMRI IC1 showed a positive relationship to naming and verbal fluency performance for patients with extensive left hemispheric damage (Griffis et al., 2017b). Given that these regions show up-regulated task-evoked activity during early recovery, but show normalized levels of task-evoked activation in chronic patients who successfully recover (Heiss et al., 1999; Saur et al., 2006), we speculated that the beneficial relationship between activity in these regions and language task performance for patients with extensive left hemispheric damage might reflect the maintenance of early compensatory mechanisms into the chronic recovery phase (Griffis et al., 2017b). Accordingly, patients with left posterior lesions may also be less likely than patients with frontal or sub-cortical lesions to restore function in canonical language networks during recovery, and have been reported to continue to show task-evoked activation in right fronto-temporal networks at later stages of recovery than frontal and sub-cortical patients (Heiss et al., 1999). While increased activation of right posterior temporo-parietal areas has also been reported in patients with extensive left hemispheric damage (Sims et al., 2016), our previous study that explicitly investigated relationships between lesion size and right hemispheric activations in these patients did not find evidence for a relationship between activation in these regions and lesion size (Griffis et al., 2017b). Thus, a second potential explanation for the relationship captured in joint IC1 is that decreased task-driven segregation in patients with left temporo-parietal damage reflects compensation rather than inter-network dysregulation. However, it is also possible that these are not mutually exclusive. For example, diminished task-specific suppression of activity in right fronto-temporo-parietal networks following damage to hub regions such as the left angular gyrus might facilitate compensation via these networks during task performance, although this should be regarded as speculation.

4.2 Limitations

In this study, we attempted to build upon and extend our previous hypothesis-driven studies of this patient sample by utilizing data-driven multivariate analyses to characterize links between complex patterns of task-evoked brain activation and regional left hemispheric tissue preservation. Despite the various advantages of data-driven approaches to studying

such complex relationships, they are nonetheless exploratory (Sui et al., 2014). It is therefore important to emphasize that confirmatory studies designed to test pre-specified and theory-driven hypotheses are a necessary next step in developing a thorough understanding of structure-function relationships in chronic left hemispheric stroke. In the previous section, we presented two broad hypotheses regarding the potential nature of the observed effects, and while they provide direction for future studies in this area, we stress that they must be considered speculative until they can be tested by confirmatory studies.

In addition, because this study only included chronic patients, it cannot be concluded whether the observed activation patterns reflect the initial preservation vs. eventual restoration of network function. Further, it is unclear to what extent the observed effects might be influenced by pre-stroke differences among patients in brain structure (Forkel et al., 2014), and longitudinal studies are necessary to interrogate such possibilities.

Another limitation common to most lesion studies is that the sMRI components include heterogeneous anatomical areas that fall within a given branch of the left middle cerebral artery territory. The locations of strokes are not random, but reflect the vascular distribution of the brain (Richardson et al., 2012; Rorden et al., 2007; Rorden and Karnath, 2004). Given that ICA is a data-driven technique that decomposes MRI data into statistically independent spatial patterns, some correspondence between the decomposed structural data and the vasculature of the LMCA territory is to be expected. Notably, while structural components identified by previous studies using similar techniques (i.e. jICA) to study structure-function relationships in chronic stroke patients have often featured large swaths of tissue spanning multiple lobes (e.g. Abel et al., 2015; Robson et al., 2016), the sMRI ICs identified in this study were relatively spatially constrained. Further, the voxel contributions to each component were not uniform, indicating that specific areas contributed more to each component than to others (Figure 3).

We note that performance data on clinical aphasia batteries with domain-specific sub-tests (e.g. Western Aphasia Battery) were not available for all of the patients, and the language data were collected for relatively high-level language tasks. While they may be ideal to fully characterize the patients, detailed aphasia assessments were not necessary to accomplish the aim of the current study. Importantly, the available data included performance on the in-scanner semantic task-of-interest, and also included performance on out-of-scanner tasks that emphasize distinct language domains. Given that it is not uncommon for studies that do collect detailed clinical assessments to not incorporate them fully or even at all in the analyses, but rather focus on a sub-test, in-scanner task, or other task of interest (Abel et al., 2014; Fridriksson et al., 2012, 2010; Laura M Skipper-Kallal et al., 2017a, 2017b; Specht et al., 2009), we do not consider this limitation particularly problematic.

Finally, the tractography analyses utilized group-averaged data from healthy individuals, and are essentially qualitative. While similar approaches have been used by previous studies (Turken and Dronkers et al., 2011; Mirman et al., 2015; Fridriksson et al., 2013; Harvey and Schnur, 2015; Griffis et al., 2017a), this must be acknowledged as a limitation. Further, while QSDR, which is an extension of generalized q-sampling imaging (GQI), is superior to traditional diffusion tensor imaging (DTI) approaches for resolving crossing fibers (Yeh and

Tseng, 2011), other model-based approaches may perform best in this regard (Lichenstein et al., 2016; Wilkins et al., 2015).

5. Summary and Conclusions

In conclusion, we found the preservation of left posterior temporo-parietal cortices and the underlying deep white matter to be associated with greater semantic task-evoked activation in default mode and peri-sylvian sub-networks of the CSN, and with lower semantic task-evoked activation in a set of right fronto-temporo-parietal areas. Patient mixing profile coefficients for both the temporo-parietal tissue preservation component and the CSN activation component positively predicted performance on in-scanner and out-of-scanner language tasks. Exploratory fiber tracking analyses found evidence to suggest that lesions affecting left temporo-parietal areas may have a disproportionate impact on the structural connections of the CSN, and suggest that the relationship between tissue preservation in these areas and activation in regions associated with the CSN may partially reflect the preservation of long-range structural connections. These results provide important insights into how language task-evoked activation patterns in chronic stroke patients relate to the preservation of left hemispheric structures, and provide specific hypotheses regarding structure-function relationships in this population that can motivate future studies in this area.

Supplementary Material

Refer to Web version on PubMed Central for supplementary material.

Acknowledgments

Amber Martin

Christi Banks

NIH R01 HD068488

NIH R01 NS048281

Data were provided [in part] by the Human Connectome Project, WU-Minn Consortium (Principal Investigators: David Van Essen and Kamil Ugurbil; 1U54MH091657) funded by the 16 NIH Institutes and Centers that support the NIH Blueprint for Neuroscience Research; and by the McDonnell Center for Systems Neuroscience at Washington University.

References

Abel S, Weiller C, Huber W, Willmes K. Neural underpinnings for model-oriented therapy of aphasic word production. Neuropsychologia. 2014; 57:154–165. DOI: 10.1016/j.neuropsychologia.2014.03.010 [PubMed: 24686092]

Abel S, Weiller C, Huber W, Willmes K, Specht K. Therapy-induced brain reorganization patterns in aphasia. Brain. 2015; 138:1097–112. DOI: 10.1093/brain/awv022 [PubMed: 25688082]

Aickin M, Gensler H. Adjusting for multiple testing when reporting research results: The Bonferroni vs Holm methods. Am J Public Health. 1996; 86:726–728. DOI: 10.2105/AJPH.86.5.726 [PubMed: 8629727]

Baldassarre A, Ramsey L, Hacker CL, Callejas A, Astafiev SV, Metcalf NV, Zinn K, Rengachary J, Snyder AZ, Carter AR, Shulman GL, Corbetta M. Large-scale changes in network interactions as a

physiological signature of spatial neglect. Brain. 2014; 137:3267–3283. DOI: 10.1093/brain/awu297 [PubMed: 25367028]

Bartolomeo P, de Schotten MT. Let the left brain know what the right brain does: Inter-hemispheric compensation of functional deficits after brain damage. Neuropsychologia. 2016; :1–6. DOI: 10.1016/j.neuropsychologia.2016.06.016

Belsley, DA., Kuh, E., Welsch, RE. Regression Diagnostics Identifying Influential Data and Sources of Collinearity. New York: John Wiley & Sons; 1980.

Benjamini Y, Hochberg Y. Controlling the False Discovery Rate: A Practical and Powerful Approach to Multiple Testing. J R Stat Soc Ser B. 1995; 57:289–300.

Binder J, Desai R. The neurobiology of semantic memory. Trends Cogn Sci. 2011; 15:527–536. DOI: 10.1016/j.tics.2011.10.001 [PubMed: 22001867]

Binder J, Desai R, Graves W, Conant L. Where is the semantic system? A critical review and meta-analysis of 120 functional neuroimaging studies. Cereb Cortex. 2009; 19:2767–2796. DOI: 10.1093/cercor/bhp055 [PubMed: 19329570]

Binder J, Frost J, Hammeke T, Bellgowan P, Rao S, Cox R. Conceptual processing during the conscious resting state: A functional MRI study. J Cogn Neurosci. 1999; 11:80–93. DOI: 10.1162/089892999563265 [PubMed: 9950716]

Binder J, Frost J, Hammeke T, Cox R, Rao S, Prieto T. Human brain language areas identified by functional magnetic resonance imaging. J Neurosci. 1997; 17:353–362. [PubMed: 8987760]

Binder J, Swanson S, Hammeke T, Sabsevitz D. A comparison of five fMRI protocols for mapping speech comprehension systems. Epilepsia. 2008; 49:1980–1997. DOI: 10.1111/j.1528-1167.2008.01683.x [PubMed: 18513352]

Blank SC, Bird H, Turkheimer F, Wise RJS. Speech production after stroke: The role of the right pars opercularis. Ann Neurol. 2003; 54:310–320. DOI: 10.1002/ana.10656 [PubMed: 12953263]

Blasi V, Young AC, Tansy AP, Petersen SE, Snyder AZ, Corbetta M. Word retrieval learning modulates right frontal cortex in patients with left frontal damage. Neuron. 2002; 36:159–170. DOI: 10.1016/S0896-6273(02)00936-4 [PubMed: 12367514]

Buckner RL, Sepulcre J, Talukdar T, Krienen FM, Liu H, Hedden T, Andrews-Hanna JR, Sperling RA, Johnson KA. Cortical hubs revealed by intrinsic functional connectivity: mapping, assessment of stability, and relation to Alzheimer's disease. J Neurosci. 2009; 29:1860–1873. DOI: 10.1523/JNEUROSCI.5062-08.2009 [PubMed: 19211893]

Calhoun VD, Adali T, Giuliani NR, Pekar JJ, Kiehl KA, Pearlson GD. Method for multimodal analysis of independent source differences in schizophrenia: Combining gray matter structural and auditory oddball functional data. Hum Brain Mapp. 2006; 27:47–62. DOI: 10.1002/hbm.20166 [PubMed: 16108017]

Catani M, Dell'Acqua F, Bizzi A, Forkel SJ, Williams SC, Simmons A, Murphy DG, Thiebaut de Schotten M. Beyond cortical localization in clinico-anatomical correlation. Cortex. 2012; 48:1262–1287. DOI: 10.1016/j.cortex.2012.07.001 [PubMed: 22995574]

Cole MW, Bassett DS, Power JD, Braver TS, Petersen SE. Intrinsic and task-evoked network architectures of the human brain. Neuron. 2014; 83:238–251. DOI: 10.1016/j.neuron.2014.05.014 [PubMed: 24991964]

Correa NM, Li YO, Adali T, Calhoun VD. Canonical Correlation Analysis for Feature-Based Fusion of Biomedical Imaging Modalities and Its Application to Detection of Associative Networks in Schizophrenia. IEEE J Sel Top Signal Process. 2008; 2:998–1007. DOI: 10.1109/JSTSP.2008.2008265 [PubMed: 19834573]

Crinion JT, Leff AP. Recovery and treatment of aphasia after stroke: functional imaging studies. Curr Opin Neurol. 2007; 20:667–673. DOI: 10.1097/WCO.0b013e3282f1c6fa [PubMed: 17992087]

Daselaar SM, Huijbers W, Eklund K, Moscovitch M, Cabeza R. Resting-state functional connectivity of ventral parietal regions associated with attention reorienting and episodic recollection. Front Hum Neurosci. 2013; 7:38.doi: 10.3389/fnhum.2013.00038 [PubMed: 23440005]

Donnelly KM, Allendorfer JB, Szaflarski JP. Right hemispheric participation in semantic decision improves performance. Brain Res. 2011; 1419:105–116. DOI: 10.1016/j.brainres.2011.08.065 [PubMed: 21937029]

Eaton KP, Szaflarski JP, Altaye M, Ball AL, Kissela BM, Banks C, Holland SK. Reliability of fMRI for studies of language in post-stroke aphasia subjects. Neuroimage. 2008; 41:311–22. DOI: 10.1016/j.neuroimage.2008.02.033 [PubMed: 18411061]

Eldaief MC, McMains S, Hutchison RM, Halko MA, Pascual-Leone A. Reconfiguration of Intrinsic Functional Coupling Patterns Following Circumscribed Network Lesions. Cereb Cortex. 2016; :bhw139.doi: 10.1093/cercor/bhw139

Forkel SJ, Thiebaut de Schotten M, Dell'Acqua F, Kalra L, Murphy DGM, Williams SCR, Catani M. Anatomical predictors of aphasia recovery: a tractography study of bilateral perisylvian language networks. Brain. 2014; 137:2027–39. DOI: 10.1093/brain/awu113 [PubMed: 24951631]

Fridriksson J, Bonilha L, Baker JM, Moser D, Rorden C. Activity in preserved left hemisphere regions predicts anomia severity in aphasia. Cereb Cortex. 2010; 20:1013–9. DOI: 10.1093/cercor/bhp160 [PubMed: 19687294]

Fridriksson J, Richardson JD, Fillmore P, Cai B. Left hemisphere plasticity and aphasia recovery. Neuroimage. 2012; 60:854–63. DOI: 10.1016/j.neuroimage.2011.12.057 [PubMed: 22227052]

Friston KJ, Holmes AP, Worsley KJ, Poline JP, Frith CD, Frackowiak RSJ. Statistical parametric maps in functional imaging: A general linear approach. Hum Brain Mapp. 1995; 2:189–210. DOI: 10.1002/hbm.460020402

Genovese CR, Lazar NA, Nichols T. Thresholding of statistical maps in functional neuroimaging using the false discovery rate. Neuroimage. 2002; 15:870–8. DOI: 10.1006/nimg.2001.1037 [PubMed: 11906227]

Geranmayeh F, Leech R, Wise RJS. Network dysfunction predicts speech production after left hemisphere stroke. Neurology. 2016; 86:1296–1305. DOI: 10.1212/WNL.0000000000002537

Griffis J, Allendorfer J, Szaflarski J. Voxel-based Gaussian naïve Bayes classification of ischemic stroke lesions in individual T1-weighted MRI scans. J Neurosci Methods. 2016; 257:97–108. DOI: 10.1016/j.jneumeth.2015.09.019 [PubMed: 26432931]

Griffis J, Nenert R, Allendorfer J, Szaflarski J. Damage to white matter bottlenecks contributes to language impairments after left hemispheric stroke. NeuroImage Clin. 2017a; doi: 10.1016/j.nicl.2017.02.019

Griffis J, Nenert R, Allendorfer J, Vannest J, Holland S, Dietz A, Szaflarski J. The Canonical Semantic Network Supports Residual Language Function in Chronic Post-Stroke Aphasia. Hum Brain Mapp. 2017b; 38:1636–1658. DOI: 10.1002/hbm.23476 [PubMed: 27981674]

Hamilton RH, Chrysikou EG, Coslett B. Mechanisms of aphasia recovery after stroke and the role of noninvasive brain stimulation. Brain Lang. 2011; 118:40–50. DOI: 10.1016/j.bandl.2011.02.005 [PubMed: 21459427]

Harvey DY, Schnur TT. Distinct loci of lexical and semantic access deficits in aphasia: Evidence from voxel-based lesion-symptom mapping and diffusion tensor imaging. Cortex. 2015; 67:37–58. DOI: 10.1016/j.cortex.2015.03.004 [PubMed: 25880795]

He BJ, Snyder AZ, Vincent JL, Epstein A, Shulman GL, Corbetta M. Breakdown of functional connectivity in frontoparietal networks underlies behavioral deficits in spatial neglect. Neuron. 2007; 53:905–18. DOI: 10.1016/j.neuron.2007.02.013 [PubMed: 17359924]

Heiss W, Kessler J, Thiel A, Ghaemi M, Karbe H. Differential capacity of left and right hemispheric areas for compensation of poststroke aphasia. Ann Neurol. 1999; 45:430–438. DOI: 10.1002/1531-8249(199904)45:4<430::AID-ANA3>3.0.CO;2-P [PubMed: 10211466]

Heiss W, Thiel A. A proposed regional hierarchy in recovery of post-stroke aphasia. Brain Lang. 2006; 98:118–23. DOI: 10.1016/j.bandl.2006.02.002 [PubMed: 16564566]

Honey C, Sporns O. Predicting human resting-state functional connectivity from structural connectivity. Proceedings of the National Academy of Sciences. 2009; 106:1–6.

Ivanova MV, Isaev DY, Dragoy OV, Akinina Yu S, Petryshevskii AG, Fedina ON, Shklovsky VM, Dronkers NF. Diffusion-tensor imaging of major white matter tracts and their role in language processing in aphasia. Cortex. 2016; :1–17. DOI: 10.1016/j.cortex.2016.04.019

Kaplan, E., Goodglass, H., Weintraub, S. The Boston naming test. Philadeplphia, PA: Lippincott, Williams, and Wilkins; 2001.

Karbe H, Thiel A, Weber-luxenburger G, Kessler J, Heiss W. Brain Plasticity in Poststroke Aphasia: What Is the Contribution of the Right Hemisphere? Brain Lang. 1998; 230:215–230.

Kim KK, Karunanayaka P, Privitera MD, Holland SK, Szaflarski JP. Semantic association investigated with functional MRI and independent component analysis. Epilepsy Behav. 2011; 20:613–622. DOI: 10.1016/j.yebeh.2010.11.010 [PubMed: 21296027]

Kozora E, Cullum CM. Generative naming in normal aging: Total output and qualitative changes using phonemic and semantic constraints. Clin Neuropsychol. 1995; 9:313–320.

Lau JKL, Humphreys GW, Douis H, Balani A, Bickerton W, Rotshtein P. The relation of object naming and other visual speech production tasks:A large scale voxel-based morphometric study. NeuroImage Clin. 2015; 7:463–475. DOI: 10.1016/j.nicl.2015.01.015 [PubMed: 25685713]

Lezak, MD., Howieson, DB., Loring, DW., Hannay, JH., Fischer, JS. Neuropsychological assessment. 3. Oxford University Press; New York: 1995.

Li YO, Adali T, Calhoun VD. Estimating the number of independent components for functional magnetic resonance imaging data. Hum Brain Mapp. 2007; 28:1251–1266. DOI: 10.1002/hbm.20359 [PubMed: 17274023]

Lichenstein SD, Bishop JH, Verstynen TD, Yeh FC. Diffusion capillary phantom vs. human data: Outcomes for reconstruction methods depend on evaluation medium. Front Neurosci. 2016; 10:1–13. DOI: 10.3389/fnins.2016.00407 [PubMed: 26858586]

Liu J, Pearlson G, Windemuth A, Ruano G, Perrone-Bizzozero NI, Calhoun V. Combining fMRI and SNP data to investigate connections between brain function and genetics using parallel ICA. Hum Brain Mapp. 2009; 30:241–255. DOI: 10.1002/hbm.20508 [PubMed: 18072279]

Martino J, Da Silva-Freitas R, Caballero H, Marco De Lucas E, Garcia-Porrero JA, Vazquez-Barquero A. Fiber dissection and diffusion tensor imaging tractography study of the temporoparietal fiber intersection area. Neurosurgery. 2013; 72doi: 10.1227/NEU.0b013e318274294b

Mehta S, Grabowski TJ, Trivedi Y, Damasio H. Evaluation of voxel-based morphometry for focal lesion detection in individuals. Neuroimage. 2003; 20:1438–1454. DOI: 10.1016/S1053-8119(03)00377-X [PubMed: 14642458]

Meier TB, Wildenberg JC, Liu J, Chen J, Calhoun VD, Biswal BB, Meyerand ME, Birn RM, Prabhakaran V. Parallel ICA identifies sub-components of resting state networks that covary with behavioral indices. Front Hum Neurosci. 2012; 6:1–14. DOI: 10.3389/fnhum.2012.00281 [PubMed: 22279433]

Mirman D, Chen Q, Zhang Y, Wang Z, Faseyitan OK, Coslett HB, Schwartz MF. Neural organization of spoken language revealed by lesion–symptom mapping. Nat Commun. 2015; 6:6762.doi: 10.1038/ncomms7762 [PubMed: 25879574]

Poldrack, Ra. The future of fMRI in cognitive neuroscience. Neuroimage. 2012; 62:1216–20. DOI: 10.1016/j.neuroimage.2011.08.007 [PubMed: 21856431]

Ramsey LE, Siegel JS, Lang CE, Strube M, Shulman GL, Corbetta M. Behavioural clusters and predictors of performance during recovery from stroke. Nat Hum Behav. 2017; 1:38.doi: 10.1038/s41562-016-0038

Richardson JD, Fillmore P, Rorden C, LaPointe LL, Fridriksson J. Re-establishing Broca's initial findings. Brain Lang. 2012; 123:125–130. DOI: 10.1016/j.bandl.2012.08.007 [PubMed: 23058844]

Robson H, Specht K, Beaumont H, Parkes LM, Sage K, Lambon Ralph MA, Zahn R. Arterial spin labelling shows functional depression of non-lesion tissue in chronic Wernicke's aphasia. Cortex. 2016; :1–12. DOI: 10.1016/j.cortex.2016.11.002

Rorden C, Karnath HO. Using human brain lesions to infer function: a relic from a past era in the fMRI age? Nat Rev Neurosci. 2004; 5:813–819. DOI: 10.1038/nrn1521 [PubMed: 15378041]

Rorden C, Karnath HO, Bonilha L. Improving lesion-symptom mapping. J Cogn Neurosci. 2007; 19:1081–1088. DOI: 10.1162/jocn.2007.19.7.1081 [PubMed: 17583985]

Sanjuan A, Price CJ, Mancini L, Josse G, Grogan A, Yamamoto AK, Geva S, Leff AP, Yousry TA, Seghier ML. Automated identification of brain tumors from single MR images based on segmentation with refined patient-specific priors. Front Neurosci. 2013; 7:1–12. DOI: 10.3389/fnins.2013.00241 [PubMed: 23386807]

Saur D, Hartwigsen G. Neurobiology of language recovery after stroke: lessons from neuroimaging studies. Arch Phys Med Rehabil. 2012; 93:S15–25. DOI: 10.1016/j.apmr.2011.03.036 [PubMed: 22202187]

Saur D, Lange R, Baumgaertner A, Schraknepper V, Willmes K, Rijntjes M, Weiller C. Dynamics of language reorganization after stroke. Brain. 2006; 129:1371–84. DOI: 10.1093/brain/awl090 [PubMed: 16638796]

Seghier ML, Ramlackhansingh A, Crinion J, Leff AP, Price CJ. Lesion identification using unified segmentation-normalisation models and fuzzy clustering. Neuroimage. 2008; 41:1253–1266. DOI: 10.1016/j.neuroimage.2008.03.028 [PubMed: 18482850]

Sims JA, Kapse K, Glynn P, Sandberg C, Tripodis Y, Kiran S. The relationships between the amount of spared tissue, percent signal change, and accuracy in semantic processing in aphasia. Neuropsychologia. 2016; 84:113–126. DOI: 10.1016/j.neuropsychologia.2015.10.019 [PubMed: 26775192]

Skipper-Kallal LM, Lacey EH, Xing S, Turkeltaub PE. Right Hemisphere Remapping of Naming Functions Depends on Lesion Size and Location in Poststroke Aphasia. Neural Plast. 2017a; 2017

Skipper-Kallal LM, Lacey EH, Xing S, Turkeltaub PE. Functional activation independently contributes to naming ability and relates to lesion site in post-stroke aphasia. Hum Brain Mapp. 2017b; 0doi: 10.1002/hbm.23504

Skipper-Kallal LM, Mirman D, Olson IR. Converging evidence from fMRI and aphasia that the left temporoparietal cortex has an essential role in representing abstract semantic knowledge. Cortex. 2015; 69:104–120. DOI: 10.1016/j.cortex.2015.04.021 [PubMed: 26026619]

Slotnick SD, Moo LR, Segal JB, Hart J. Distinct prefrontal cortex activity associated with item memory and source memory for visual shapes. Cogn Brain Res. 2003; 17:75–82. DOI: 10.1016/S0926-6410(03)00082-X

Specht K, Zahn R, Willmes K, Weis S, Holtel C, Krause BJ, Herzog H, Huber W. Joint independent component analysis of structural and functional images reveals complex patterns of functional reorganisation in stroke aphasia. Neuroimage. 2009; 47:2057–2063. DOI: 10.1016/j.neuroimage.2009.06.011 [PubMed: 19524049]

Stephen JM, Coffman BA, Jung RE, Bustillo JR, Aine CJ, Calhoun VD. Using joint ICA to link function and structure using MEG and DTI in schizophrenia. Neuroimage. 2013; 83:418–430. DOI: 10.1016/j.neuroimage.2013.06.038 [PubMed: 23777757]

Sui J, Adali T, Pearlson G, Yang H, Sponheim SR, White T, Calhoun VD. A CCA+ICA based model for multi-task brain imaging data fusion and its application to schizophrenia. Neuroimage. 2010; 51:123–134. DOI: 10.1016/j.neuroimage.2010.01.069 [PubMed: 20114081]

Sui J, Huster R, Yu Q, Segall JM, Calhoun VD. Function-structure associations of the brain: Evidence from multimodal connectivity and covariance studies. Neuroimage. 2014; 102:11–23. DOI: 10.1016/j.neuroimage.2013.09.044 [PubMed: 24084066]

Sui J, Pearlson G, Caprihan A, Adali T, Kiehl KA, Liu J, Yamamoto J, Calhoun VD. Discriminating schizophrenia and bipolar disorder by fusing fMRI and DTI in a multimodal CCA+ joint ICA model. Neuroimage. 2011; 57:839–855. DOI: 10.1016/j.neuroimage.2011.05.055 [PubMed: 21640835]

Szaflarski JP, Allendorfer JB, Banks C, Vannest J, Holland SK. Recovered vs. not-recovered from post-stroke aphasia: the contributions from the dominant and non-dominant hemispheres. Restor Neurol Neurosci. 2013; 31:347–60. DOI: 10.3233/RNN-120267 [PubMed: 23482065]

Szaflarski JP, Holland SK, Jacola LM, Lindsell C, Privitera MD, Szaflarski M. Comprehensive presurgical functional MRI language evaluation in adult patients with epilepsy. Epilepsy Behav. 2008; 12:74–83. DOI: 10.1016/j.yebeh.2007.07.015 [PubMed: 17964221]

Turkeltaub PE, Coslett HB, Thomas AL, Faseyitan O, Benson J, Norise C, Hamilton RH. The right hemisphere is not unitary in its role in aphasia recovery. Cortex. 2012; 48:1179–1186. DOI: 10.1016/j.cortex.2011.06.010 [PubMed: 21794852]

Turkeltaub PE, Messing S, Norise C, Hamilton RH. Are networks for residual language function and recovery consistent across aphasic patients? Neurology. 2011; 76:1726–34. DOI: 10.1212/WNL.0b013e31821a44c1 [PubMed: 21576689]

Turken AU, Dronkers NF. The neural architecture of the language comprehension network: converging evidence from lesion and connectivity analyses. Front Syst Neurosci. 2011; 5:1.doi: 10.3389/fnsys.2011.00001 [PubMed: 21347218]

Uddin LQ, Kelly AM, Biswal BB, Castellanos FX, Milham MP. Functional connectivity of default mode network components: correlation, anticorrelation, and causality. Hum Brain Mapp. 2009; 30:625–37. DOI: 10.1002/hbm.20531 [PubMed: 18219617]

Uddin LQ, Supekar K, Amin H, Rykhlevskaia E, Nguyen DA, Greicius MD, Menon V. Dissociable connectivity within human angular gyrus and intraparietal sulcus: evidence from functional and structural connectivity. Cereb Cortex. 2010; 20:2636–46. DOI: 10.1093/cercor/bhq011 [PubMed: 20154013]

van Oers CMM, Vink M, van Zandvoort MJE, van der Worp HB, de Haan EHF, Kappelle LJ, Ramsey NF, Dijkhuizen RM. Contribution of the left and right inferior frontal gyrus in recovery from aphasia. A functional MRI study in stroke patients with preserved hemodynamic responsiveness. Neuroimage. 2010; 49:885–93. DOI: 10.1016/j.neuroimage.2009.08.057 [PubMed: 19733673]

Wager TD, Keller MC, Lacey SC, Jonides J. Increased sensitivity in neuroimaging analyses using robust regression. Neuroimage. 2005; 26:99–113. DOI: 10.1016/j.neuroimage.2005.01.011 [PubMed: 15862210]

Wilke M, de Haan B, Juenger H, Karnath HO. Manual, semi-automated, and automated delineation of chronic brain lesions: a comparison of methods. Neuroimage. 2011; 56:2038–46. DOI: 10.1016/j.neuroimage.2011.04.014 [PubMed: 21513805]

Wilkins B, Lee N, Gajawelli N, Law M, Lepore N. Fiber estimation and tractography in diffusion MRI: Development of simulated brain images and comparison of multi-fiber analysis methods at clinical b-values. Neuroimage. 2015; 109:341–356. DOI: 10.1016/j.neuroimage.2014.12.060 [PubMed: 25555998]

Winhuisen L, Thiel A, Schumacher B, Kessler J, Rudolf J, Haupt WF, Heiss WD. Role of the contralateral inferior frontal gyrus in recovery of language function in poststroke aphasia: a combined repetitive transcranial magnetic stimulation and positron emission tomography study. Stroke. 2005; 36:1759–63. DOI: 10.1161/01.STR.0000174487.81126.ef [PubMed: 16020770]

Xu Y, Lin Q, Han Z, He Y, Bi Y. Intrinsic functional network architecture of human semantic processing: Modules and hubs. Neuroimage. 2016; 132:542–555. DOI: 10.1016/j.neuroimage.2016.03.004 [PubMed: 26973170]

Yeh FC, Panesar S, Fernandes D, Meola A, Yoshino M, Fernandez-Miranda JC, Vettel J, Verstynen T. A Population-Based Atlas Of The Macroscale Structural Connectome In The Human Brain. 2017; doi: 10.1101/136473

Yeh FC, Wedeen VJ, Tseng WYI. Generalized q-Sampling Imaging. IEEE Trans Med Imaging. 2010; 29:1626–1635. DOI: 10.1109/TMI.2010.2045126 [PubMed: 20304721]

Yeh FC, Tseng WYI. NTU-90: A high angular resolution brain atlas constructed by q-space diffeomorphic reconstruction. Neuroimage. 2011; 58:91–99. DOI: 10.1016/j.neuroimage.2011.06.021 [PubMed: 21704171]

Yeh FC, Verstynen TD, Wang Y, Fernández-Miranda JC, Tseng WYI. Deterministic diffusion fiber tracking improved by quantitative anisotropy. PLoS One. 2013; 8:1–16. DOI: 10.1371/journal.pone.0080713

Highlights

- We use data fusion analyses to link structure and function in chronic stroke.
- Semantic task activation is linked to sparing of left temporo-parietal areas.
- Left temporo-parietal lesions may disrupt semantic network connections.
- Data fusion provides insights into structure-function relationships after stroke.

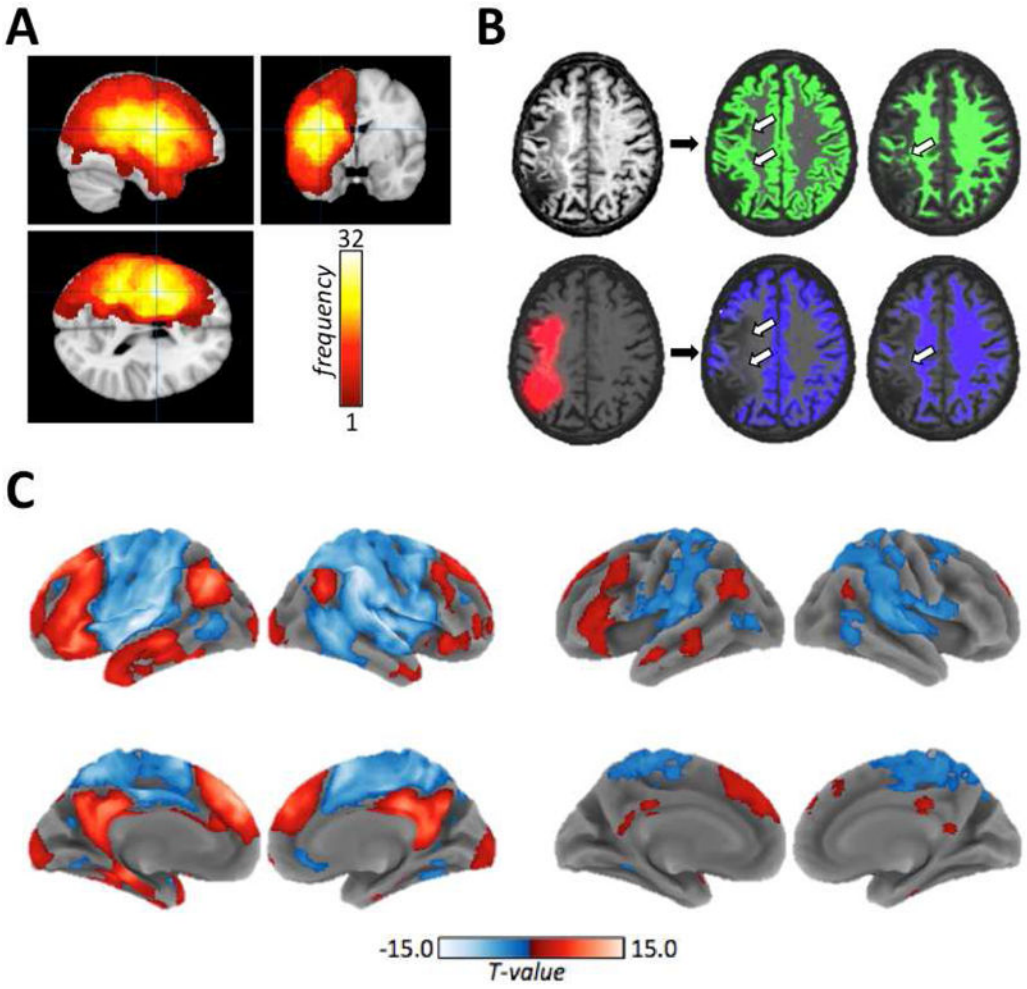

Figure 1.

A. Lesion frequencies for all 43 patients are shown on orthogonal slices of a template brain. Color bar values indicate the number of patients with lesions at each voxel, and the voxels are centered on the voxel with the highest lesion frequency (max=32). **B.** Top – a template normalized T1-weighted image from a single patient (left) is shown along with the normalized (un-smoothed and un-thresholded) GM and WM segmentations (shown in green) obtained using standard tissue priors. Arrows indicate lesion voxels that were erroneously classified as intact tissue. Bottom – the same template normalized image is shown overlaid with extra lesion prior (shown in red), along with the GM and WM segmentations (shown in blue) obtained using the modified segmentation. Previously misclassified voxels are now correctly assigned to the extra tissue class, and are no longer apparent in the GM/WM TPMs as indicated by the arrows. **C.** Group-level activation (*t*-contrast) maps for the control (left) and stroke (right) groups obtained using a standard mass-univariate analysis of the semantic decision minus tone decision contrast. Maps are thresholded at $p<0.01$ at the voxel-level and FWE$p<0.05$ at the cluster-level. Red indicates activations associated with semantic decisions relative to tone decisions, and blue indicates de-activations.

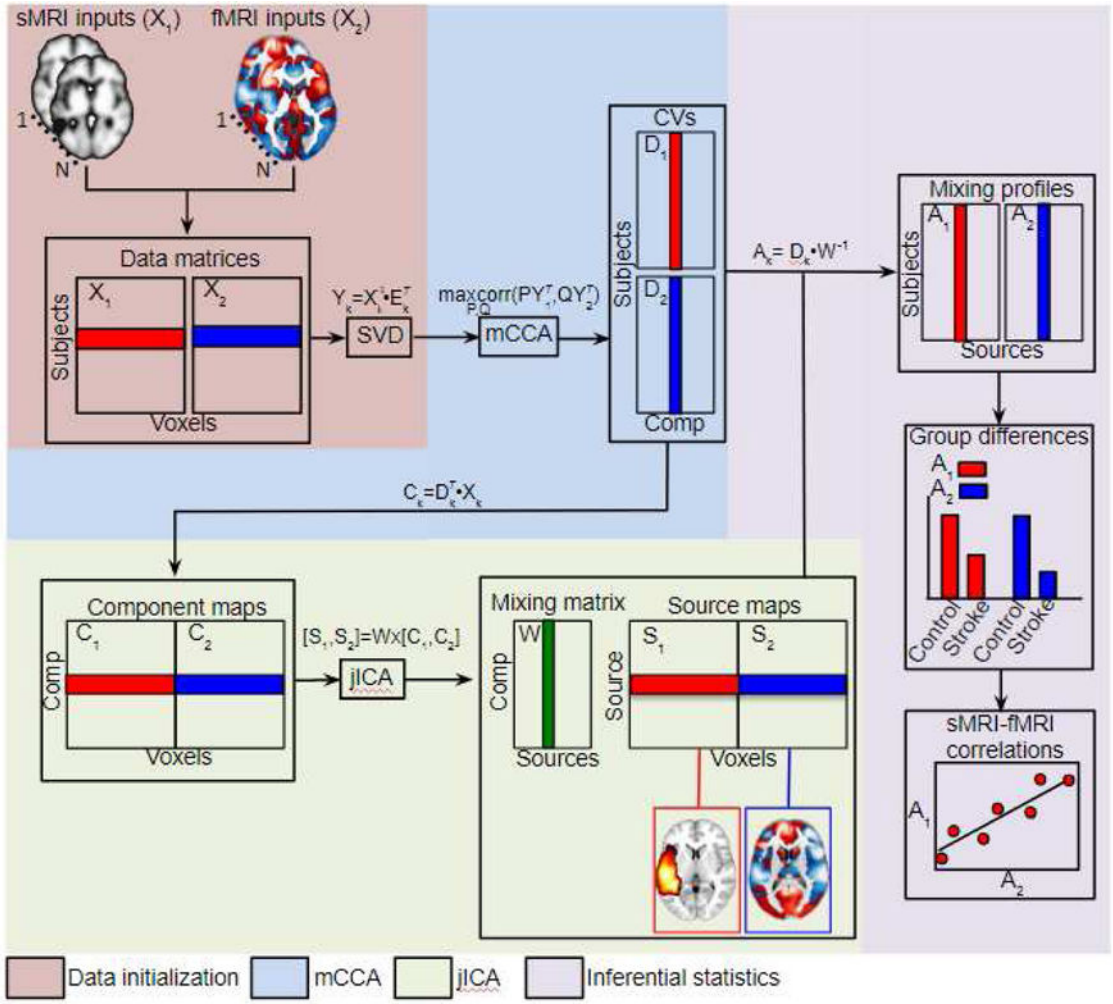

Figure 2. Schematic illustration of mCCA+jICA

The diagram illustrates the mCCA+jICA pipeline. Data from each modality are first re-shaped into subject-by-voxel data matrices (X_1,X_2), pre-processed, and dimension-reduced via SVD. mCCA is then used to obtain canonical variates (D_1,D_2) and associated components (C_1,C_2) by finding the sets of basis vectors (P,Q) that maximize the correlations between the projections of (Y_1,Y_2). The components are concatenated into a single data matrix and input into the joint ICA to obtain the joint source matrix (S_1,S_2) and the mixing matrix (W). The mixing matrix obtained from joint ICA and the canonical variates obtained from mCCA are used to compute modality-specific mixing profiles (A_1,A_2) for each joint component. Comparisons of the mixing profiles between patient and control groups are used to select joint components of interest. Correlations between the sMRI and fMRI mixing profiles for each joint component provide an estimate of the strength of the structure-function relationship captured in each joint component. The source matrix is used to reconstruct spatial maps quantifying voxel-level contributions to the joint components of interest.

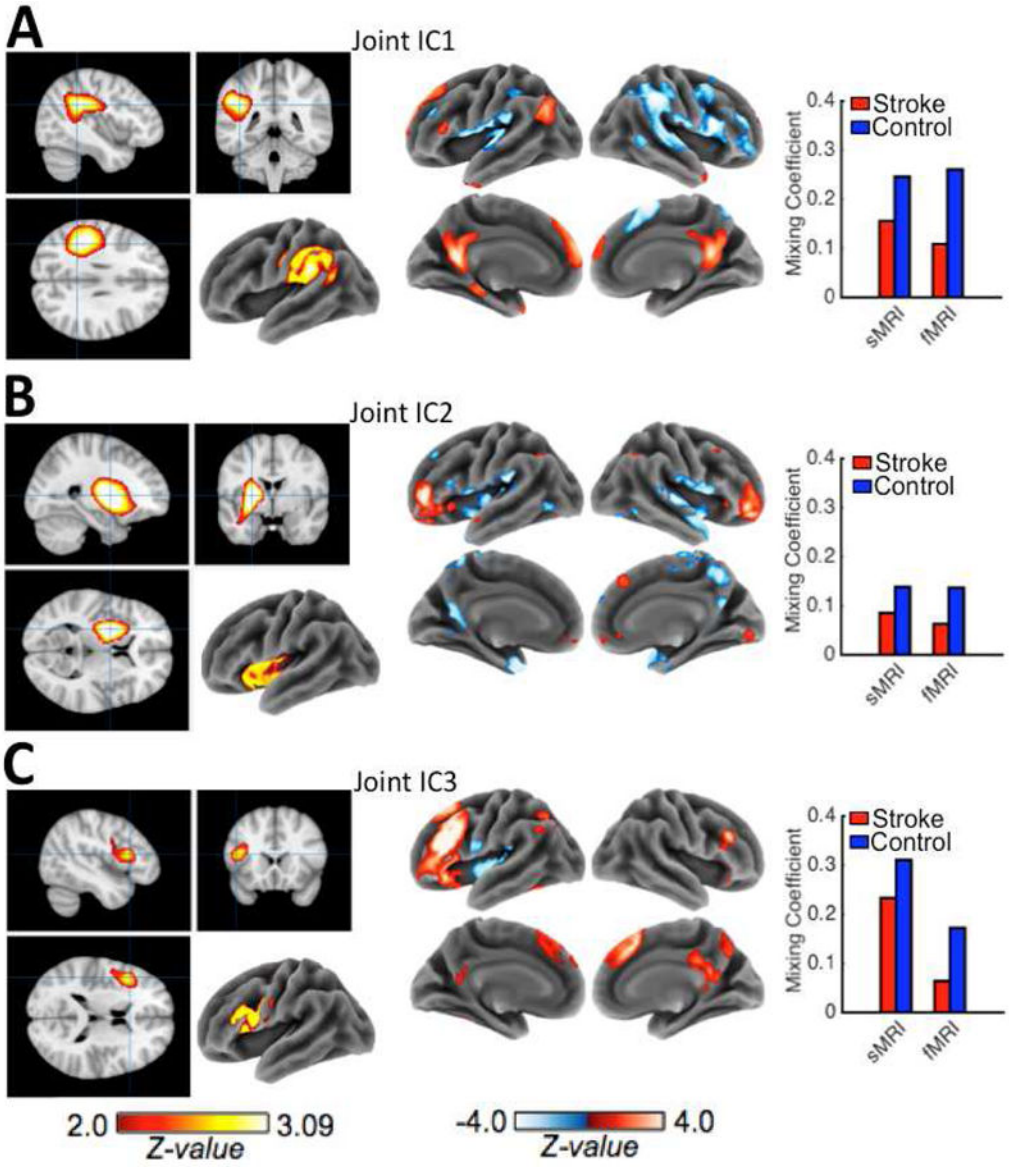

Figure 3.

A–C. Z-scaled (|Z| > 2.0) back-reconstructed maps for the sMRI (left) and fMRI (right) components of each group-differentiating joint IC are shown along with bar graphs of the mean sMRI and fMRI mixing coefficients (loadings) from stroke patients (red) and controls (blue) on each group-differentiating joint IC. Patient loadings were significantly (FWEp<0.05) lower than control loadings for all 3 group-differentiating joint ICs, indicating that these components were less represented in the patient data than in the control data.

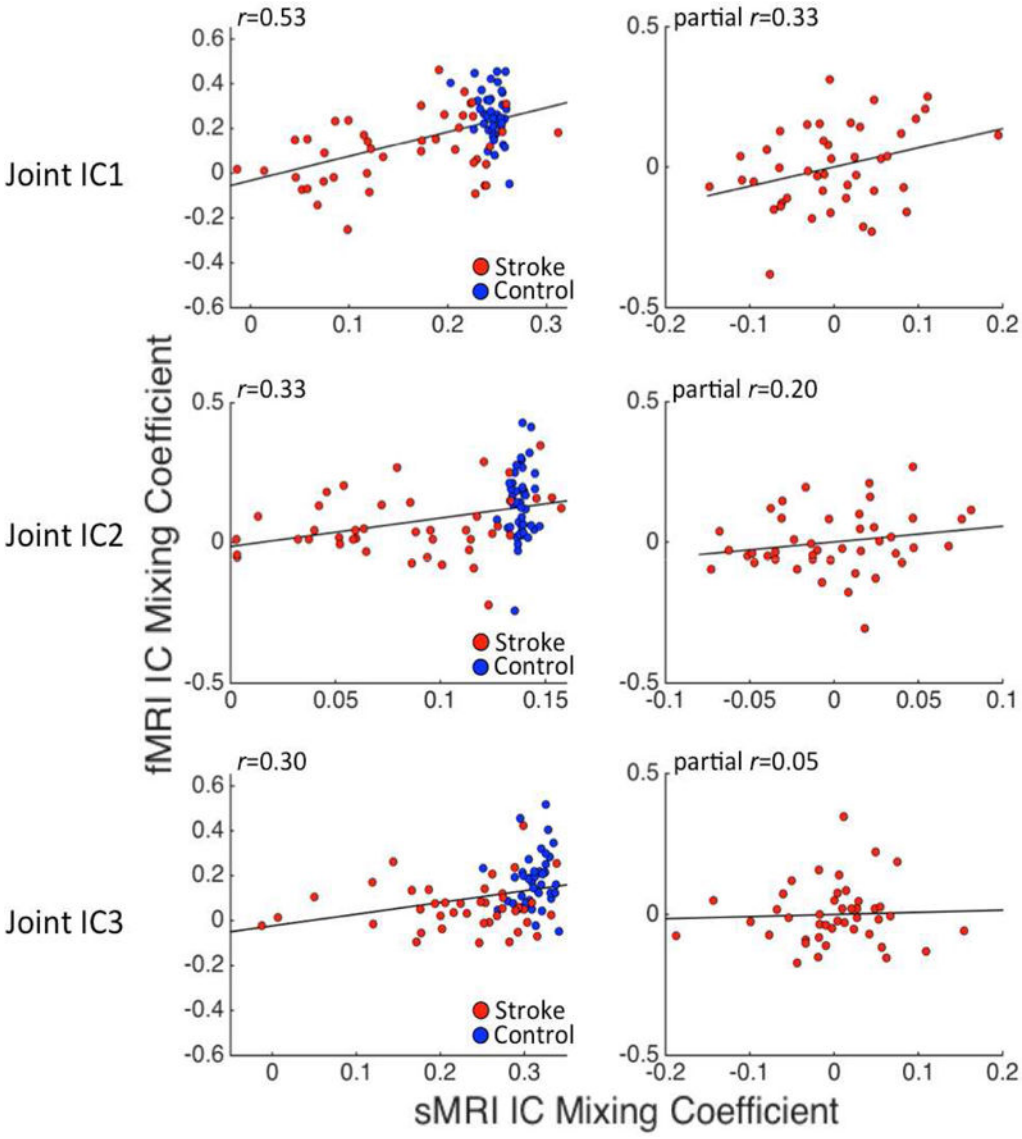

Figure 4.

Scatterplots illustrate correlations between sMRI (x-axis) and fMRI (y-axis) mixing coefficients for the group-differentiating joint ICs identified by mCCA+jICA. Plots on the left show the un-adjusted correlations computed across all participants (i.e. both healthy controls and stroke patients). The plots on the right show partial correlations (controlling for left hemispheric brain volume) computed using only data from the stroke patient group. Stroke cases are shown in red, and control cases are shown in blue.

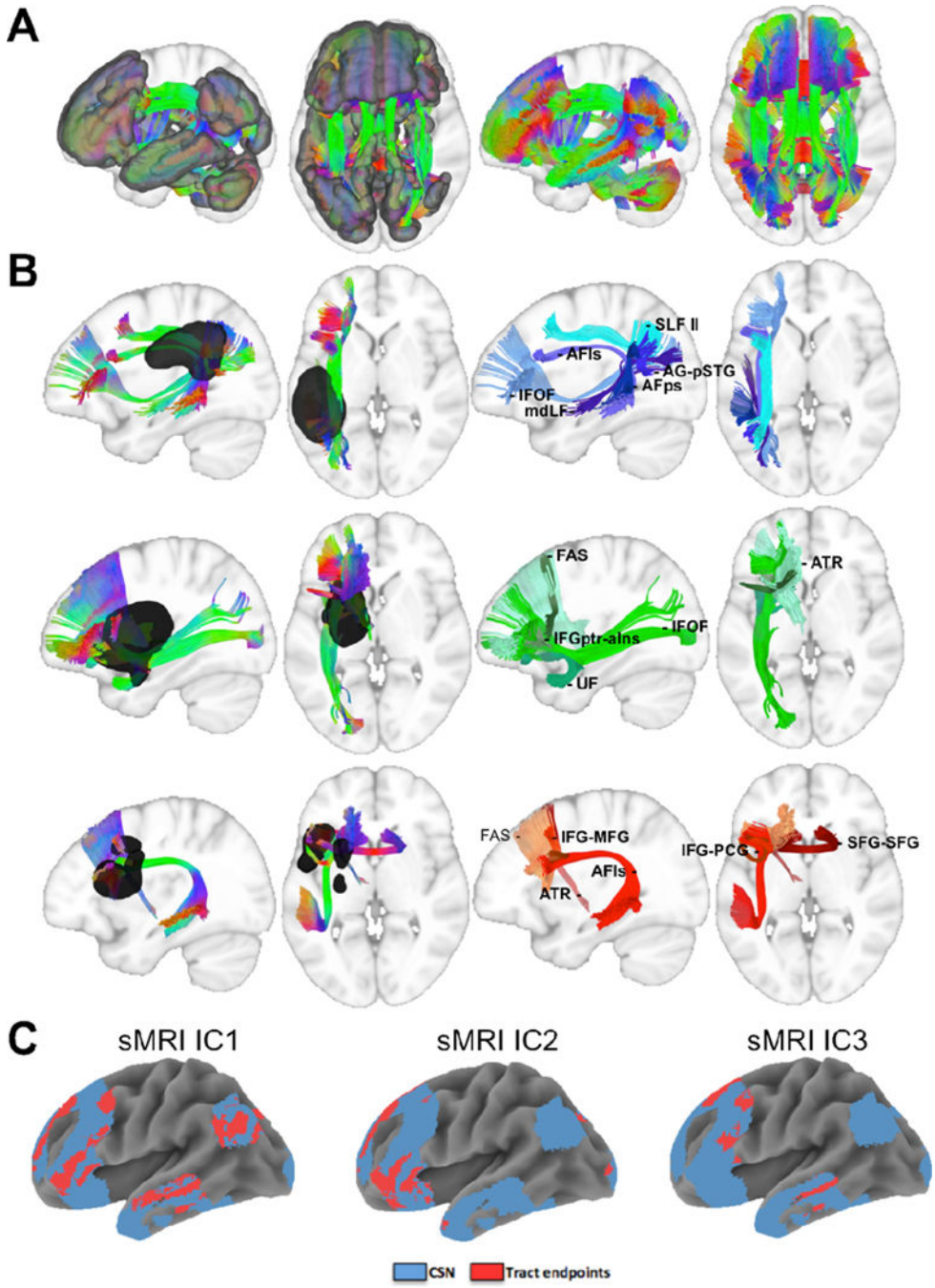

Figure 5.

A. Fibers connecting CSN regions are overlaid on sagittal and axial slices of a template brain with (left) and without (right) the semantic network ROI. **B.** Fibers connecting semantic network regions that pass through locations corresponding to sMRI IC1 (top), sMRI IC2 (middle), and sMRI IC3 (bottom) are overlaid on sagittal and axial slices of a template brain with (left) and without (right) the sMRI IC ROIs. **C.** Tract endpoints (red) are overlaid along with the CSN (blue) to illustrate the CSN regions with connections passing through each sMRI IC. *SLF II – superior longitudinal fasciculus II; AFls – arcuate*

fasciculus long segment; AFps – arcuate fasciculus posterior segment; IFOF – inferior fronto-occipital fasciculus; mdLF – middle longitudinal fasciculus; AG-pSTG – angular gyrus and posterior superior temporal gyrus; ATR – anterior thalamic radiations; UF – uncinate fasciculus; FAS – frontal aslant; IFGptr-aIns – inferior frontal gyrus pars triangularis and anterior insula; IFG-MFG – inferior frontal gyrus and middle frontal gyrus; IFG-PCG – inferior frontal gyrus and precentral gyrus; SFG-SFG – superior frontal gyrus and superior frontal gyrus

Table 1

Participant demographics and language test scores

Group	N	Age	Sex	EHI	Lesion volume (ml)	LH brain volume (ml)	SD	Verbal Fluency	Naming
Patients	43	53 (15)	25 M	0.85 (0.43)	105.24 (76.29)	549.17 (85.90)	47.28 (22.59)	14.42 (12.33)	35.77 (20.80)
Controls	43	54 (14)	23 M	0.80 (0.41)	N/A	712.98 (43.24)	69.16 (19.09)	47.81 (10.66)	57.54 (2.67)

*Mean (Standard deviation) are shown for age/handedness; M-Male; EHI-Edinburgh Handedness Inventory; LH-Left Hemisphere; SD-Semantic Decision

Table 2

Regressions of patient behavioral scores on loadings for selected components

sMRI Model (SD Correct) R^2=0.22 FWEp=0.03			
Predictor	**ß**	**t**	**P (FDRp)**
sMRI IC1	**0.41**	**2.74**	**0.009 (0.02)**
sMRI IC2	0.06	0.38	0.71 (0.77)
sMRI IC3	−0.01	−0.06	0.95 (0.95)
sMRI Model (Verbal Fluency) R^2=0.38, FWEp=0.001			
Predictor	**ß**	**t**	**P (FDRp)**
sMRI IC1	**0.38**	**2.86**	**0.006 (0.02)**
sMRI IC2	**0.29**	**2.19**	**0.03 (0.045)**
sMRI IC3	**0.36**	**2.8**	**0.007 (0.02)**
sMRI Model (Naming) R^2=0.25, FWEp=0.02			
Predictor	**ß**	**t**	**P (FDRp)**
sMRI IC1	**0.44**	**2.8**	**0.007 (0.02)**
sMRI IC2	0.14	0.88	0.38 (0.49)
sMRI IC3	0.28	1.87	0.07 (0.10)
fMRI Model (SD Correct) R^2 =0.38, FWEp=0.003			
Predictor	**ß**	**t**	**P (FDRp)**
fMRI IC1	**0.31**	**2.32**	**0.026 (0.04)**
fMRI IC2	**0.31**	**2.34**	**0.025 (0.04)**
fMRI IC3	**0.45**	**3.4**	**0.002 (0.02)**
fMRI Model (Verbal Fluency) R^2=0.48, FWEp<0.001			
Predictor	**ß**	**t**	**P (FDRp)**
fMRI IC1	**0.34**	**2.86**	**0.007 (0.02)**
fMRI IC2	0.08	0.63	0.53 (0.60)
fMRI IC3	**0.55**	**4.72**	**0.00003 (<0.001)**
fMRI Model (Naming) R^2 =0.28, FWEp=0.01			
Predictor	**ß**	**t**	**P (FDRp)**
fMRI IC1	**0.36**	**2.36**	**0.02 (0.04)**
fMRI IC2	0.1	0.63	0.53 (0.60)
fMRI IC3	**0.41**	**2.79**	**0.008 (0.02)**

Note: Significant models and predictors are indicated by bold text.